Monthly Notices
of the
ROYAL ASTRONOMICAL SOCIETY

Mon. Not. R. Astron. Soc. **403,** 2167–2175 (2010) doi:10.1111/j.1365-2966.2010.16262.x

Observations of the quiescent X-ray transients GRS 1124–684 (=GU Mus) and Cen X-4 (=V822 Cen) taken with ULTRACAM on the VLT⋆

T. Shahbaz,[1]† V. S. Dhillon,[2] T. R. Marsh,[3] J. Casares,[1] C. Zurita[1] and P. A. Charles[4]

[1]*Instituto de Astrofísica de Canarias, 38200 La Laguna, Tenerife, Spain*
[2]*Department of Physics and Astronomy, University of Sheffield, Sheffield S3 7RH*
[3]*Department of Physics, University of Warwick, Coventry CV4 7AL*
[4]*South African Astronomical Observatory, PO Box 9, Observatory 7935, Cape Town, South Africa*

Accepted 2009 December 29. Received 2009 December 29; in original form 2009 March 20

ABSTRACT

We present high time-resolution multicolour optical observations of the quiescent X-ray transients GRS 1124–684 (=GU Mus) and Cen X-4 (=V822 Cen) obtained with ULTRACAM. Superimposed on the secondary stars' ellipsoidal modulation in both objects are large flares on time-scales of 30–60 min as well as several distinct rapid flares on time-scales of a few minutes, most of which show further variability and unresolved structure. Not significant quasi-periodic oscillations are observed and the power density spectra of GRS 1124–684 and Cen X-4 can be described by a power law. From the colour–colour diagrams of the flare events, for GRS 1124–684 we find that the flares can be described by hydrogen gas with a density of $N_{\rm H} \sim 10^{24}$ nucleons cm^{-2}, a temperature of $\sim$8000 K and arising from a radius of $\sim$0.3 R$_{\odot}$. Finally we compile the values for the transition radius (the radius of the hot advection-dominated accretion flow) estimated from quasi-periodic oscillations and/or breaks in the power density spectrum for a variety of X-ray transients in different X-ray states. As expected, we find a strong correlation between the bolometric luminosity and the transition radius.

Key words: accretion, accretion discs – binaries: close – stars: individual: GRS 1124–684 (=GU Mus) – stars: individual: Cen X-4 (=V822 Cen).

1 INTRODUCTION

X-ray transients (XRTs) are a subset of low-mass X-ray binaries that display episodic, dramatic X-ray and optical outbursts, usually lasting for several months. More than 70 per cent of XRTs are thought to contain black holes (Charles & Coe 2006). The black hole XRTs are known to exhibit five distinct X-ray spectral states, distinguished by the presence or absence of a soft blackbody component at 1 keV and the luminosity and spectral slope of emission at harder energies; these are known as the quiescent, low, intermediate, high and very high states, respectively (Tanaka & Shibazaki 1996). The quiescent and low states can mostly be explained with the advection-dominated accretion flow (ADAF) model (Narayan, McClintock & Yi 1996; Esin, McClintock & Narayan 1997). In the context of the ADAF model, properties similar to the low/hard state are expected for the quiescent state, as there is thought to be no distinction between the two except that the mass accretion rate is much higher and the size of the ADAF region is smaller for the low/hard state.

Similar to the transition between the low/hard and high/soft (thermal-dominant) states, where there is a reconfiguration of the accretion flow (Esin et al. 1997), there is also observational evidence for a state transition between the low/hard and quiescent states in that the quiescent state power-law appears softer than in the low/hard state. In both these states, the ADAF model predicts that the inner edge of the disc is truncated at some large radius, with the interior region filled by an ADAF. Strong evidence for such a truncated disc is provided by observations of XTE J1118+480 in the low/hard state during outburst (Hynes et al. 2000; Esin et al. 2001; McClintock et al. 2001; Chaty et al. 2003), where the disc has an inner radius of >55 Schwarzschild radii ($R_{\rm sch}$) and a hot optically thin plasma in the inner regions. In quiescence, the ADAF model predicts that the inner disc edge will move outwards to larger radii (Esin et al. 1997).

Variability is one of the ubiquitous characteristics of accreting black holes extending across all wavelengths. High time-resolution optical photometry of XRTs in quiescence has shown variability with a power density spectrum (PDS) very similar to those of low/hard-state XRTs, i.e. a power-law band-limited spectrum (Hynes et al. 2003a). The similarity of the PDS suggests that the optical variability could have a similar origin and might be associated with the central X-ray source. Furthermore, the presence of optical/X-ray correlations (Hynes et al. 2004) requires some

⋆Based on observations made at the European Southern Observatory, Paranal, Chile (ESO programme 075.D-0193).

†E-mail: tsh@ll.iac.es

Table 1. Log of the VLT+ULTRACAM observations.

Object	UT date starting	UT start	Exp. time (s) $u'/g'/i'$	No. of images $u'/g'/i'$	Median seeing (range) (arcsec)
GRS 1124–684	2005/05/09	23:13	5.0/5.0/5.0	4005	1.5 (1.2–2.0)
GRS 1124–684	2005/05/10	00:17	5.0/5.0/5.0	3469	1.7 (1.3–3.0)
Cen X-4	2007/06/18	01:41	6.0/3.0/3.0	3296/6579/6579/	0.6 (0.45–1.2)

association between the optical and the source of the X-rays. The origin of the break in the band-limited spectrum is not known, but it is plausible to expect that it approximately scales with the size of the inner region. A low break frequency in quiescence would then be expected, since the advective region is expected to be larger. Here we report on our high time-resolution multicolour optical observations of the black hole XRT GRS 1124–684 and the neutron star XRT Cen X-4 in quiescence. These observations are part of an ongoing campaign with ULTRACAM to obtain high time-resolution photometry of X-ray binaries (Shahbaz et al. 2003; Shahbaz et al. 2005).

2 OBSERVATIONS AND DATA REDUCTION

Multicolour photometric observations of GRS 1124–684 and Cen X-4 were obtained with ULTRACAM on the 8.2-m MELIPAL unit of the Very Large Telescope (VLT) at Paranal, Chile. The GRS 1124–684 data were taken during the nights starting 2005 May 9 and 10, whereas the Cen X-4 data were taken on the nights starting 2007 June 18 (see Table 1 for a log of the observations). ULTRACAM is an ultrafast, triple-beam CCD camera, where the light is split into three broad-band colours (blue, green and red) by two dichroics. The detectors are back-illuminated and thinned, and they are E2V frame-transfer 1024 × 1024 CCDs with a pixel scale of 0.15 arcsec pixel^{-1}. Due to the architecture of the CCDs, the dead-time is essentially zero (for further details, see Dhillon et al. 2007). Our observations were taken using the Sloan u', g' and i' filters with effective wavelengths of 3550, 4750 and 7650 Å , respectively.

The ULTRACAM pipeline reduction procedures were used to debias and flat-field the data. The same pipeline was also used to obtain light curves for GRS 1124–684, Cen X-4 and several

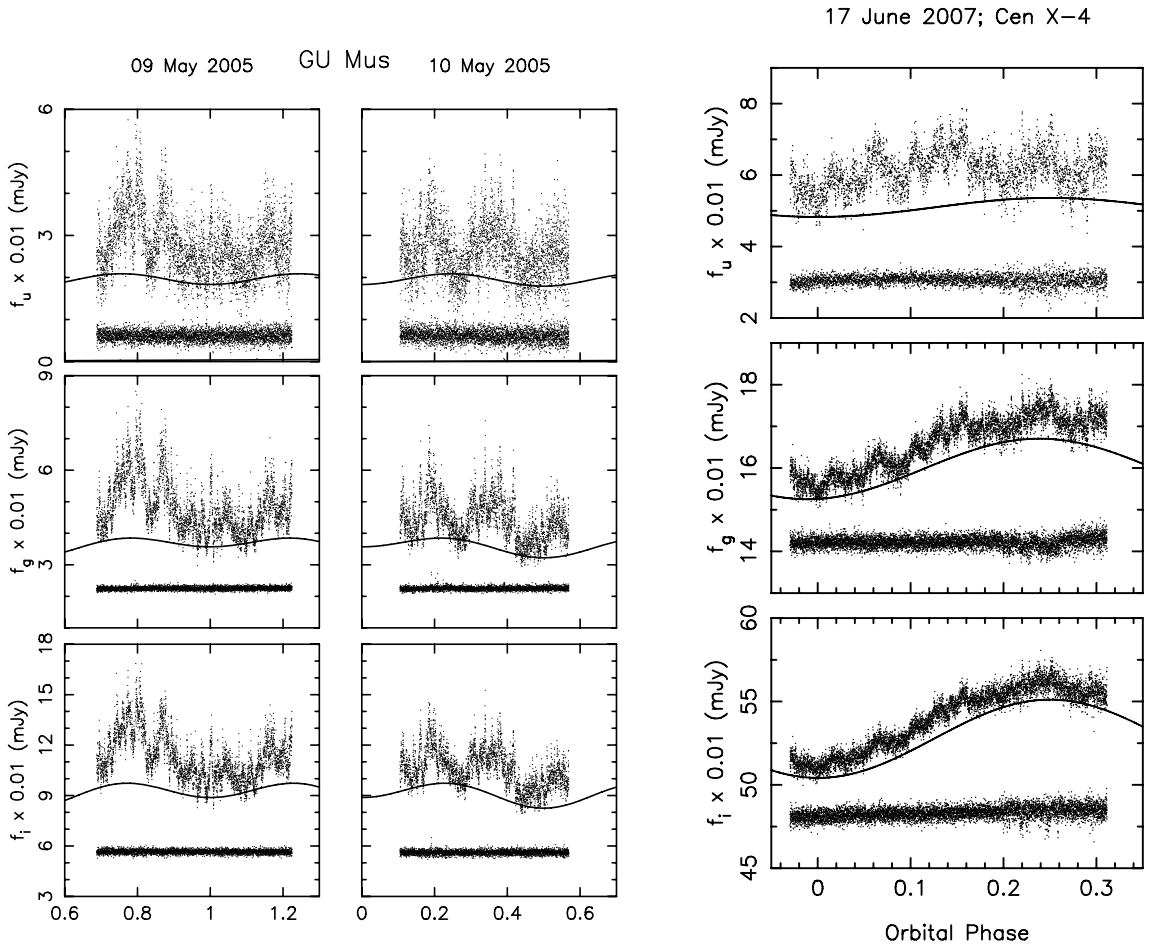

Figure 1. The de-reddened u'-, g'- and i'-band light curves of GRS 1124–684 and Cen X-4 phase-folded using the ephemeris given in Casares et al. (1997) and Torres et al. (2002), respectively; orbital phase 0.0 is defined as inferior conjunction of the secondary star. The solid line is the fitted ellipsoidal modulation. At the bottom of each panel, we also show the light curve of a comparison star of similar magnitude to the target, offset vertically for clarity.

comparison stars by extracting the counts using aperture photometry. The most reliable results were obtained using a variable aperture which scaled with the seeing. The count ratio of the target with respect to a bright local standard (which has a similar colour to our target) was then determined. The magnitude of the target was then obtained using the calibrated magnitude of the local standard. As a check of the photometry and systematics in the reduction procedure, we also extracted light curves of a faint comparison star similar in brightness to the target.

The mean magnitude of GRS 1124–684 was $u' = 21.49$, $g' = 20.65$ and $i' = 19.92$, and we estimate the photometric accuracy per exposure to be 16.4, 2.8 and 2.0 per cent for the u', g' and i' bands, respectively. For Cen X-4, the mean magnitude was $u' = 18.69$, $g' = 18.07$ and $i' = 17.27$ and we estimate the photometric accuracy per exposure to be 5.9, 0.9 and 0.6 per cent for the u', g' and i' bands, respectively. The uncertainties only reflect the 1σ statistical errors in the relative photometry.

3 SHORT-TERM VARIABILITY

The optical light curves of GRS 1124–684 and Cen X-4 (Fig. 1) show short-term variability/flares superimposed on the secondary star's weak ellipsoidal modulation. So if we want to determine the flux of the flares, these 'steady' contributions must first be removed

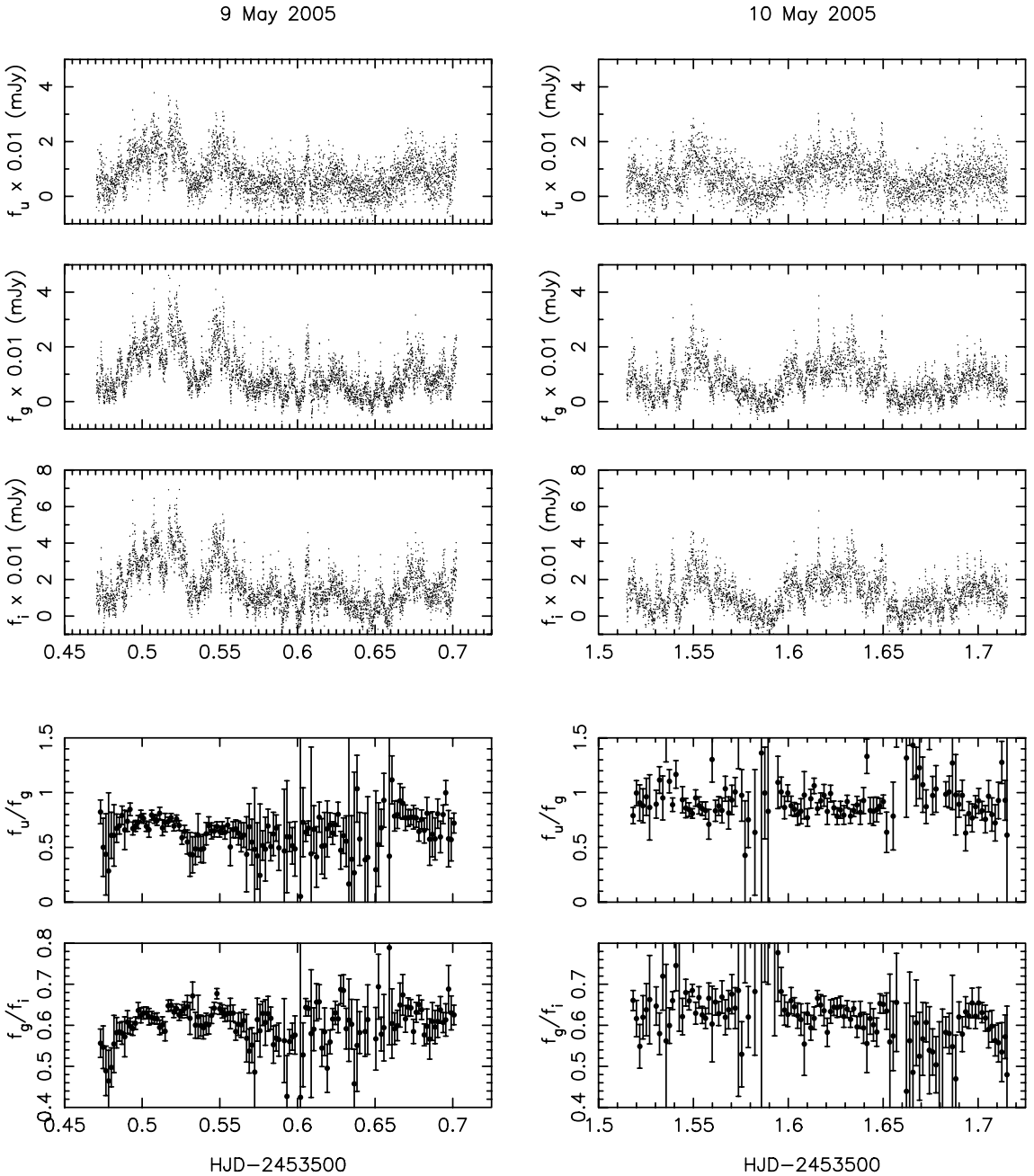

Figure 2. Top: the GRS 1124–684 flare de-reddened flux density u'-band (top panel), g'-band (middle panel) and i'-band (bottom panel) light curves obtained by subtracting a fit to the lower envelope of the light curves shown in Fig. 1. The uncertainties in the u', g' and i' light curves are 4.3×10^{-3}, 1.2×10^{-4} and 2.0×10^{-3} mJy, respectively. Bottom: the flux ratio light curves binned to a time resolution of 150 s for clarity.

from the light curves. In order to isolate the short-term variability in each band, we first de-reddened the observed magnitudes using a colour excess of $E(B-V)=0.29$ (Cheng et al. 1992) for GRS 1124–684 and $E(B-V)=0.10$ for Cen X-4 (Blair et al. 1984) and adopting the ratio $A_V/E(B-V)=3.1$ (Cardelli, Clayton & Mathis 1989), and then converted the Sloan AB magnitudes to flux density (Fukugita et al. 1996). We then fitted a double sinusoid to the lower envelope of the light curve with periods equal to the orbital period [$P_{\rm orb}=0.432\,0604$ d for GRS 1124–684 (Casares et al. 1997) and $P_{\rm orb}=0.629\,0496$ d for Cen X-4 (Torres et al. 2002)] and its first harmonic, where the phasing was fixed and the normalizations were allowed to float free. We rejected points more than 3σ above the fit and then re-fitted, repeating the procedure until no new points were rejected. For GRS 1124–684, contrary to Hynes et al. (2003a) we do not find evidence of any phase shift in the data, because one can see from Fig. 1 that orbital phase 0.0 coincides with the minimum light.

Figs 2 and 3 show the resulting light curves (after subtracting the secondary star's ellipsoidal modulation), where large flare events lasting 30–60 and 10–30 min, respectively, are clearly seen. For GRS 1124–684 what is also noticeable are numerous rapid flare events (Fig. 4), which typically last 5 min or less and which are not resolved. For both targets there are numerous short-term flares with rise/decay times of ∼3–5 min, superimposed on larger flares. For GRS 1124–684 the large flares have time-scales of 30–60 min, whereas for Cen X-4 they typically have time-scales of 10–30 min. The parameters of the flares as defined by Zurita et al. (2002) are given in Table 2.

A look at the light curves of GRS 1124–684 shows short-term flare events which seem to occur regularly. In Fig. 5, we show tick marks with representative intervals of 6.3 min. As one can see, some of the flare events seem to recur on a regular basis and the period appears to be stable on short time-scales. It is clear, however, that these events are not strictly periodic and not strong enough to show up as quasi-periodic oscillations (QPOs) in a log–log plot of the PDS (see Section 4).

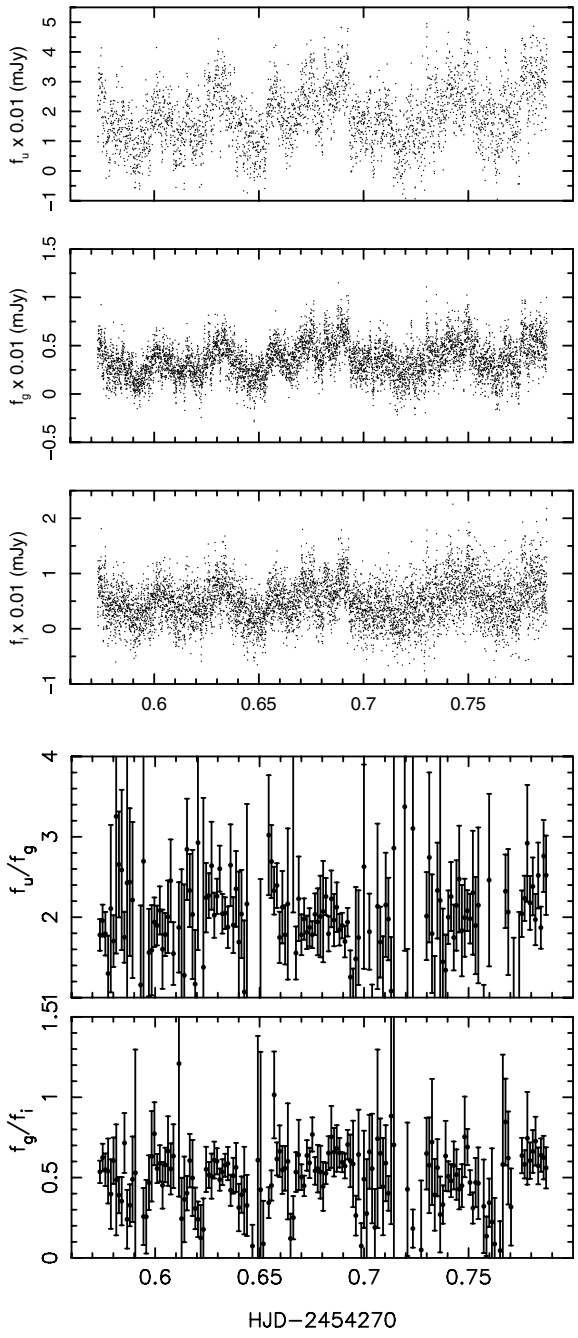

Figure 3. The top three panels show the Cen X-4 flare de-reddened flux density u'-, g'- and i'-band light curves obtained by subtracting a fit to the lower envelope of the light curves shown in Fig. 1. The uncertainties in the u', g' and i' light curves are 1.2×10^{-3}, 2.7×10^{-3} and 7.0×10^{-3} mJy, respectively. The bottom two panels show the flux ratio light curves binned to a time resolution of 135 s for clarity.

4 THE POWER DENSITY SPECTRUM

The flare light curves (i.e. after subtracting the secondary star's ellipsoidal modulation from the de-reddened light curves) of GRS 1124–684 and Cen X-4 show features which seem to be periodic. To see if this is true, we computed the PDS of the data. To compute the PDS, we detrended the data using the double sinusoid fit described in the previous section and then added the mean flux level of the data. Although the ULTRACAM sampling is perfectly uniform over short periods of time (tens of minutes), we use the Lomb–Scargle method to compute the periodograms (Press et al. 1992) with the same normalization method as is commonly used in X-ray astronomy, where the power is normalized to the fractional root mean amplitude squared per hertz (van der Klis 1994). We used the constraints imposed by the Nyquist frequency and the typical duration of each observation to limit the range of different frequencies searched.

The light curves of GRS 1124–684 and Cen X-4 show features that are present in all three bands (see Fig. 6). In order to determine the significance of possible peaks above the red-noise level, we used a Monte Carlo simulation similar to Shahbaz et al. (2005). We generated light curves with exactly the same sampling and integration times as the real data. We started with a model noise light curve generated using the method of Timmer & Koenig (1995) with a power-law index as determined from the PDS of the observed data and then added Gaussian noise using the errors derived from the photometry. We computed 5000 simulated light curves and then calculated the 95 per cent confidence level at each frequency taking into account a realistic number of independent trials (Vaughan 2005). For GRS 1124–684 and Cen X-4 the 95 per cent confidence level contour rules out any QPOs, and indeed it would seem that the PDS is dominated by red noise. Thus, the PDS of the flare light

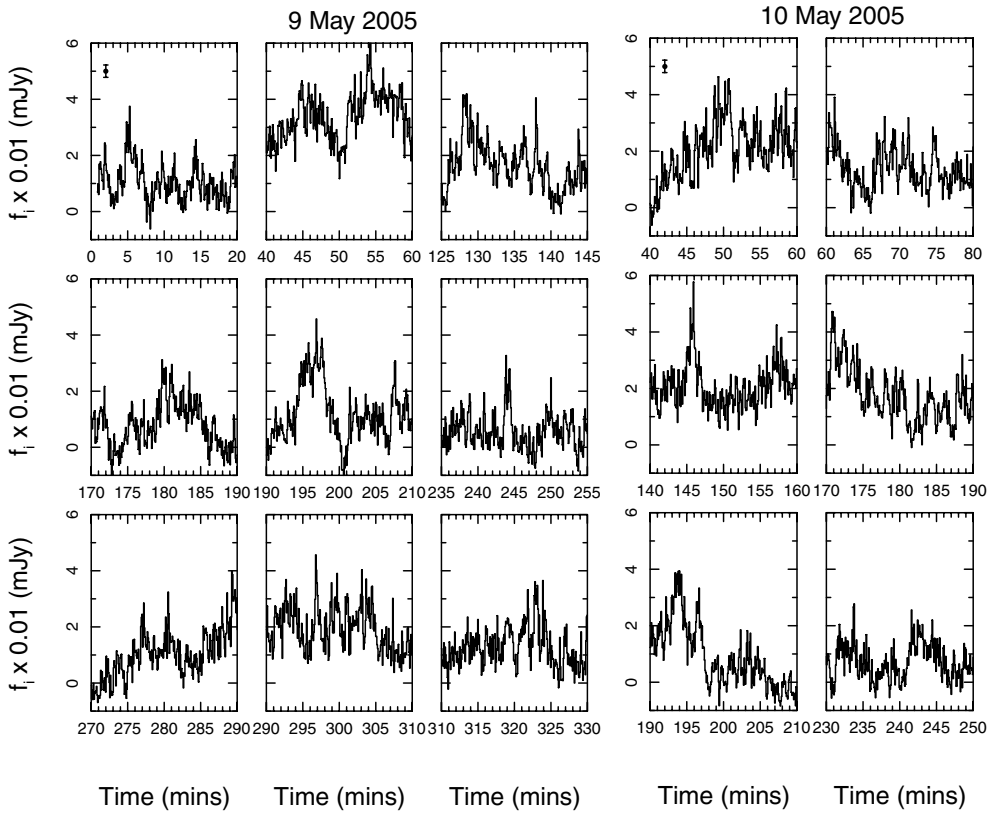

Figure 4. Detailed plot of some of the individual flares in the i'-band light curve of GRS 1124–684. Note that numerous flare events which last for a few minutes are not resolved. The solid point in the top left-hand panels marks the typical uncertainty in the data.

curve for GRS 1124–684 and Cen X-4 in each band can be described by a power-law model (see Fig. 6).

In Fig. 6 the errors in each frequency bin are determined from the standard deviation of the points within each bin, and the white noise level was subtracted by fitting the highest frequencies with a white-noise (constant) plus red-noise (power-law) model. The power-law index of the fit is also given.

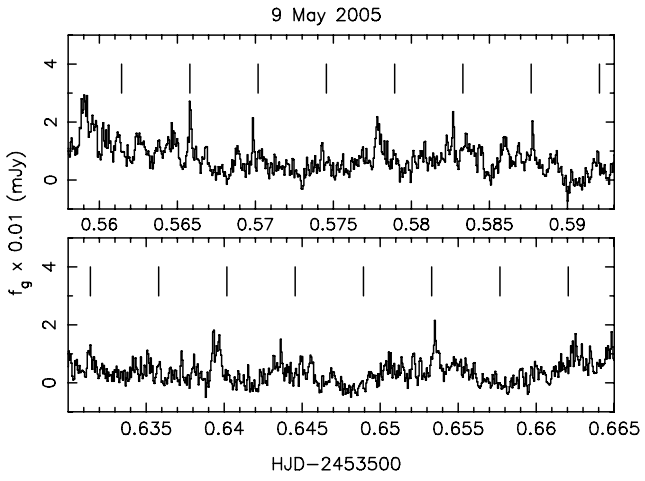

Figure 5. A close-up of the g'-band light curve of GRS 1124–684. Short-term flare events seem to be periodic, but only over a few cycles. Vertical tick marks are shown with a representative interval of 6.3 min.

5 THE ORIGIN OF THE FLARES

In an attempt to interpret the broad-band spectral properties of the flare, we compared the observed colours with the prediction for three different emission mechanisms, namely a blackbody, an optically thin layer of hydrogen and synchrotron emission. We computed the given emission spectrum and then calculated the expected flux density ratios $f_{u'}/f_{g'}$ and $f_{g'}/f_{i'}$ using the synthetic photometry package SYNPHOT (IRAF/STSDAS). Given the intrinsic model flux, we can then determine the corresponding radius of the region that produces the observed de-reddened flux at a given distance.

Fig. 7 shows the data for the flare events and the expected results for different emission models. For stellar flares the power-law index of the electron energy distribution is approximately -2 (Crosby, Aschwanden & Schmitt 1993), which corresponds to a spectral energy distribution (SED) with index $\alpha = -0.5$ ($F_\nu \propto \nu^\alpha$). However, the SED index observed in V404 Cyg ($\alpha \sim -2.0$) implies a much steeper index for the electron energy distribution (Shahbaz et al. 2003), which may not be completely implausible given the extreme conditions around a black hole. Therefore, in Fig. 7 we show the power-law model for α ranging from -2 to 2. We also show the very unlikely blackbody case, where the flares are due to blackbody radiation from a heated region of the disc's photosphere. The most likely model for a thermal flare is emission from an optically thin layer of recombining hydrogen, which is essentially the mechanism generally accepted for solar flares. We therefore determined the continuum emission spectrum of a local thermodynamic equilibrium slab of hydrogen for different baryon densities, $N_{\rm H} = 10^{21}$–10^{24} nucleons cm^{-2}, and calculated the expected flux ratios.

Table 2. Properties of the GRS 1124–684 and Cen X-4 flares. $v_{\rm obs}$ is the spectroscopic veiling, $v_d^{'}$ is the contribution to the *non-variable* disc light and $\bar{z}_f$ and σ_z are the mean flare flux and its standard deviation, respectively. $\sigma_z^* = \sigma_z/v_d^{'}$ and η is the fraction of the average veiling due to the flares (Zurita et al. 2002).

Target	Band	$v_{\rm obs}$ (per cent)	$v_d^{'}$	$\bar{z}_f$	σ_z	σ_z^*	η
GRS 1124–684	u'	94	0.92	0.387	0.25	0.27	0.27
	g'	64	0.57	0.194	0.16	0.28	0.25
	i'	15	0.04	0.133	0.11	2.8	0.78
Cen X-4	u'	60	0.48	0.312	0.13	0.27	0.39
	g'	20	0.78	0.182	0.12	0.15	0.19
	i'	5	0.70	0.042	0.005	0.007	0.06

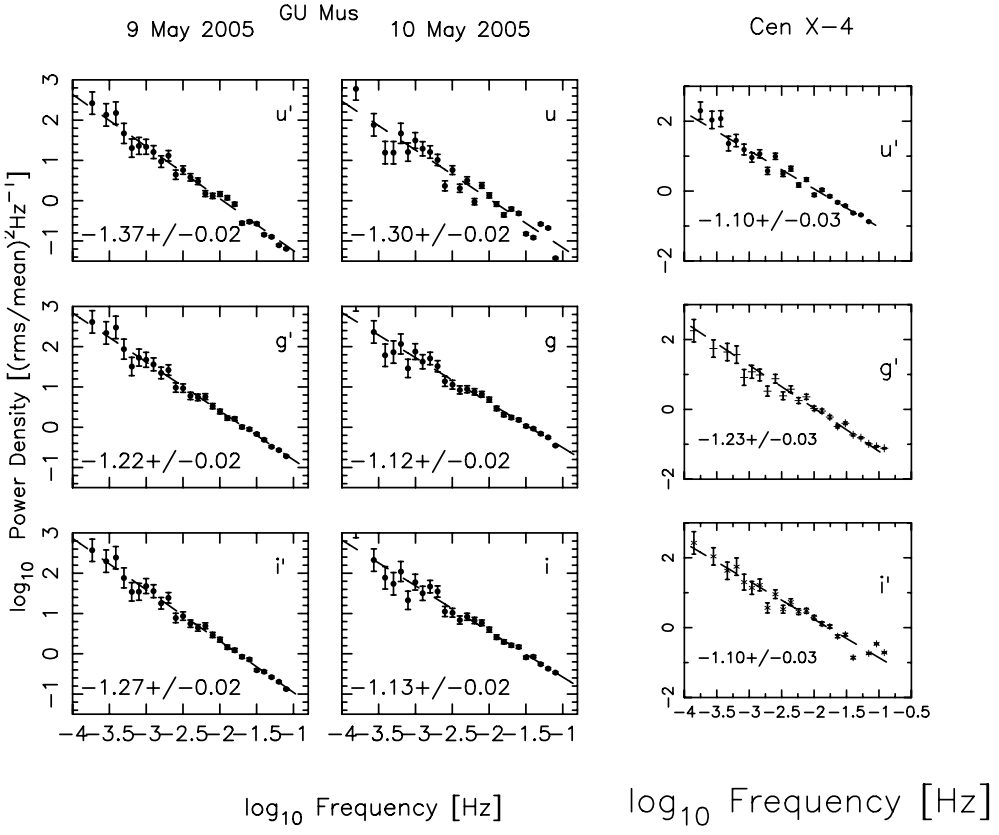

Figure 6. From top to bottom: the u', g' and i' PDS of the flare light curves of GRS 1124–684 taken on 2005 May 9 and 10 (left) and Cen X-4 taken on 2007 June 18 (right). The dashed line is a power–law fit. The slope of the power-law fit to the PDS is indicated in each panel.

For Cen X-4, the amplitudes of the flares are small and difficult to define. All we can say is that they arise from an optically thin region with $N_{\rm H} \sim 10^{21-25}$ nucleons cm^{-2}, a temperature of $\sim$8300 K and a radius of $\sim$0.06 R$_\odot$ (assuming a distance of 1.2 kpc; Chevalier et al. 1989). For GRS 1124–684, we can comment more because the flares are well defined; Fig. 7 shows the data for the best resolved small and large flares for GRS 1124–684. The flare events can be described by hydrogen gas with a density of $N_{\rm H} \sim 10^{24}$ nucleons cm^{-2} and a temperature of $\sim$8000 K, which corresponds to a radius of $\sim$0.3 R$_\odot$ (assuming a distance of 5.1 kpc; Gelino, Harrison & McNamara 2001).

6 DISCUSSION

6.1 The origin of the flares

We can compare the flares in GRS 1124–684 to the flare properties determined in other quiescent black hole XRTs. The large flares in V404 Cyg are consistent with optically thin gas with a temperature of $\sim$8000 K arising from a region with an equivalent blackbody radius of at least 2 R$_\odot$ (Shahbaz et al. 2003). One should regard the equivalent radius estimate as a lower limit, because the emission mechanism is unlikely to be blackbody. Similarly for XTE

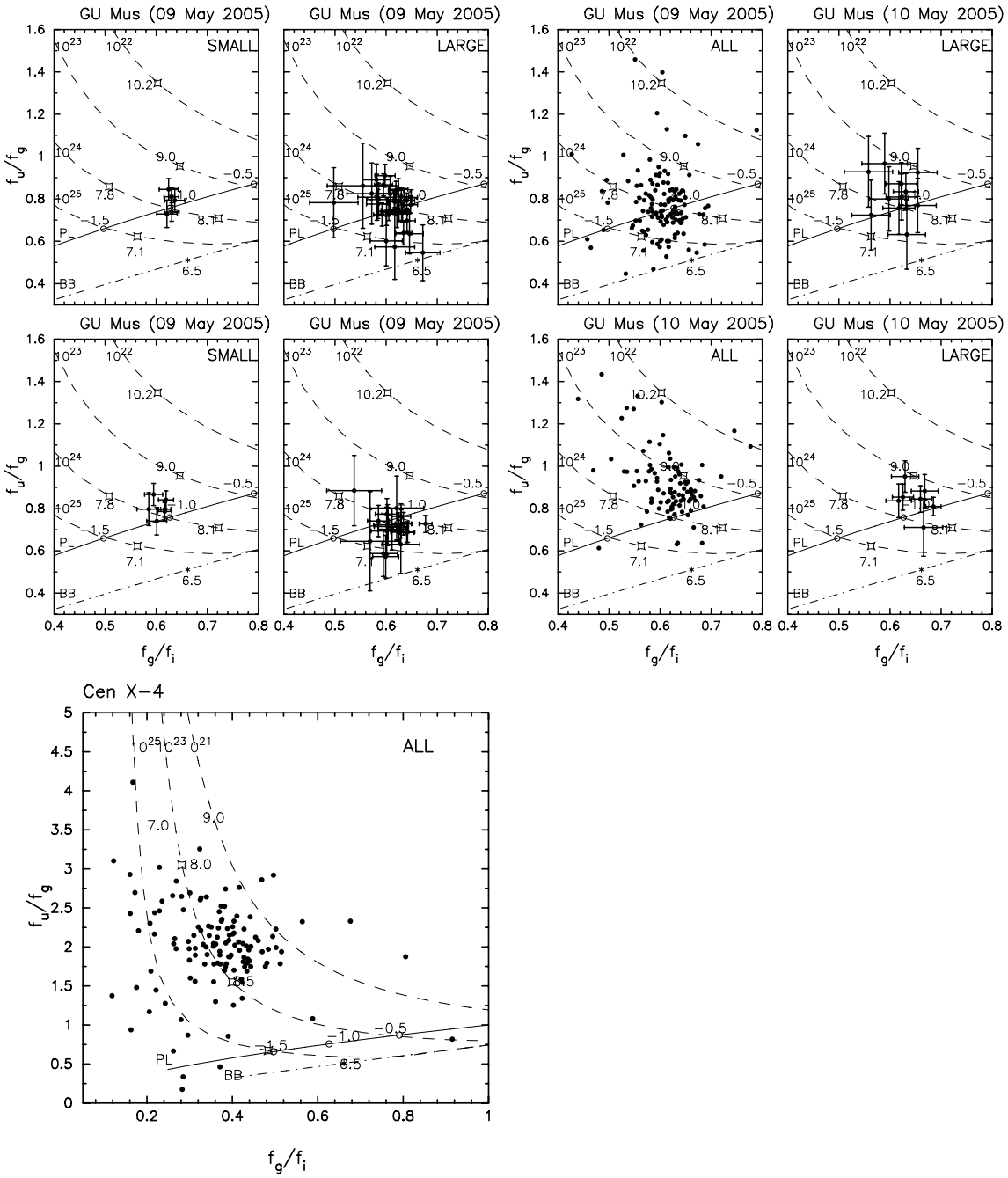

Figure 7. Colour–colour diagram for the clearest small and large flare events in GRS 1124–684 and the large flare events in Cen X-4. The panels labelled 'ALL' show all the data for that particular night, where the error bars have been removed for clarity. The dashed lines show optically thin hydrogen slab models for different column densities and the open squares show the temperature in 1000 K units. The solid line shows a power-law model ($F_\nu \propto \nu^\alpha$) with indices $\alpha = -0.5$ and -1.5 marked as open circles. The dot–dashed line is a blackbody model where the asterisk shows the colour for a temperature of 6500 K.

J1118+480, the short-term flares have a blackbody temperature of ∼3500 K and an equivalent radius of $\sim 0.10\,R_\odot$. By isolating the spectrum of the flare event in A0620–00, we found that it could be represented by optically thin gas of hydrogen with a radius of $0.04\,R_\odot$ and a temperature of 10 000–14 000 K (Shahbaz et al. 2005), which are consistent with the bright spot area and temperature. The Balmer line flux and variations in A0620–00 suggest that there are two emitting regions, the accretion disc and the accretion stream/disc impact region. The persistent emission is optically thin and during the flare events there is either an increase in temperature or the emission is more optically thick than the continuum. For GRS 1124–684 we find that the flare events reach a maximum radius of $\sim 0.3\,R_\odot$, much larger than what is observed in A0620–00 (Shahbaz et al. 2005), XTE J1118+480 (Shahbaz et al. 2004) and Cen X-4 (Section 5).

The flares GRS 1124–684 and Cen X-4 arise from various regions in the accretion disc that in total occupy 3.4 and 0.3 per cent of the disc's area, respectively. This could be from the hotspot, but the Hα Doppler maps of GRS 1124–684 and Cen X-4 do not show any evidence of a hotspot (Casares et al. 1997; Torres et al. 2002).

However, it should be noted that the optical state of quiescent transients is known to vary significantly from epoch to epoch (Cantrell et al. 2008).

6.2 The transition radius

Narayan, Barret & McClintock (1997) have shown that the X-ray observations of quiescent XRTs can be explained by a two-component accretion flow model. The geometry of the flow consists of a hot inner ADAF that extends from the black hole horizon to a transition radius $r_{\rm tr}$ and a thin accretion disc that extends from $r_{\rm tr}$ to the outer edge of the accretion disc. An ADAF has turbulent gas at all radii, with a variety of time-scales, ranging from a slow time-scale at the transition radius down to nearly the free-fall time close to the compact object. In principle, interactions between the hot inner ADAF and the cool, outer thin disc, at or near the transition radius, can be a source of optical variability, due to synchrotron emission by the hot electrons in the ADAF (Esin et al. 1997). For an ADAF the variability could be quasi-periodic and would have a characteristic time-scale given by a multiple of the Keplerian rotation period at $r_{\rm tr}$. The ADAF model also predicts that $r_{\rm tr}$ should get larger as the inner disc evaporates during the decline from outburst.

To see if there is any observational evidence for this, we have compiled the values for $r_{\rm tr}$ estimated from SED fits, QPOs and/or breaks in the PDS for a variety of XRTs in different X-ray states (see Table 3). For J1118+480 during outburst there are several estimates for $r_{\rm tr}$. The low/hard state X-ray PDS of J1118+480 (2000 April) shows a low-frequency break $f_{\rm break}$ at 23 mHz and a QPO at ∼80 mHz (Hynes et al. 2003b), which is approximately consistent with the relation observed in other sources (Wijnands & van der Klis 1999), most likely related to an instability in the accretion flow that modulates the accretion rate. The QPO frequency is most likely related to $r_{\rm tr}$, which can be a source of quasi-periodic variability and $r_{\rm tr}$ can be estimated assuming that the QPO frequency is the Keplerian rotation period at $r_{\rm tr}$. The observed QPO frequency corresponds to $r_{\rm tr} = 670$ [$t_K = 2\pi R/v_K = 2\pi(GM/R^3)^{-1/2} \sim (M/10\,{\rm M}_\odot)(r/100)^{3/2}$ s, where R is the absolute radius and r is in units of $R_{\rm sch}$].

Table 3. The transition radius for various systems.

Object	State	Method	$\log[R_{\rm tr}/R_{\rm D}]$	$\log[L_{\rm X}/L_{\rm EDD}]$	Reference
GU Mus	Ultrasoft	SED	−2.92	−0.16	Misra (1999)
J1118+480	Low/hard	SED	−1.91	−2.79	Chaty et al. (2003)
J1118+480	Low/hard	QPO	−1.72	−2.79	Hynes et al. (2003b)
J1118+480	Low/hard	PDS break	−0.77	−2.79	Hynes et al. (2003b)
J1655–40	Quiescence	Delay	−1.51	−5.25	Hameury et al. (1997)
V404 Cyg	Quiescence	QPO	−1.29	−4.89	Shahbaz et al. (2003)
A0620–00	Quiescence	PDS break	−0.05	−7.16	Hynes et al. (2003a)
J1118+480	Quiescence	PDS break	−0.07	−8.43	Shahbaz et al. (2005)

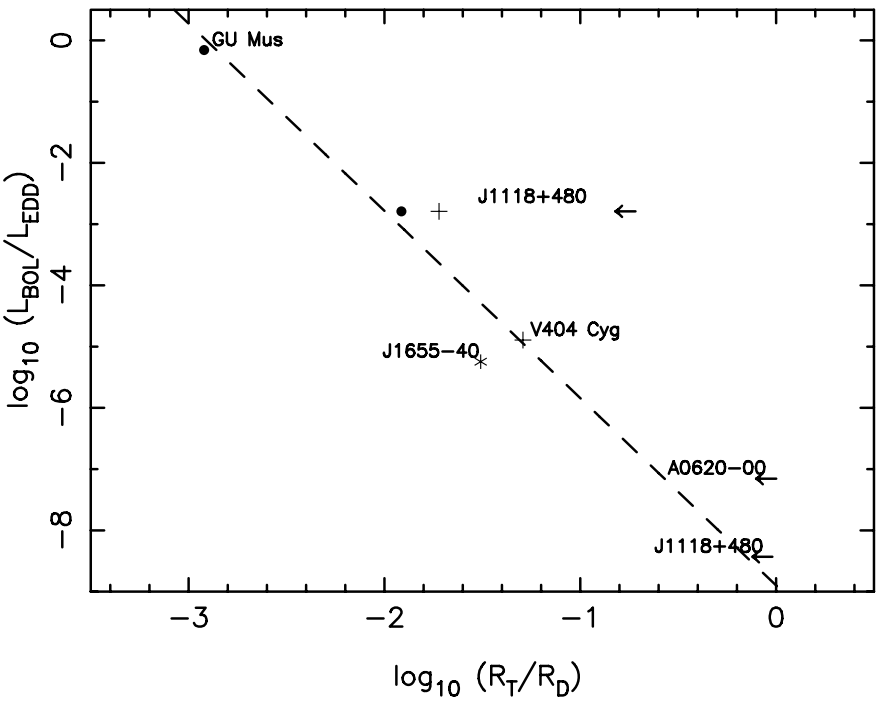

Figure 8. The transition radius (accretion disc units $R_{\rm D}$) versus bolometric luminosity (Eddington units $L_{\rm EDD}$) for a variety of XRTs in different X-ray states. The filled circles are for systems in quiescence and the crosses are for systems in the low/hard state or in outburst. The $r_{\rm tr}$ values have been determined from QPOs (crosses), breaks in the PDS (upper limit), fits to the SED (filled circles) or delays in the optical/X-ray outburst (stars): J1118+480 (Chaty et al. 2003; Shahbaz et al. 2005), A0620–00 (Hynes et al. 2003a), J1655–40 (Hameury et al. 1997), V404 Cyg (Shahbaz et al. 2003), GRS 1124–684 (Misra 1999). The X-ray luminosities are taken from Campana & Stella (2000) and the orbital parameters from Charles & Coe (2006).

For a cellular-automaton ADAF disc (Takeuchi & Mineshige 1997), the break frequency is determined by the maximum peak intensity of the X-ray shots which is on the order of the size of the advection-dominated region and corresponds to the inverse of the free-fall time-scale of the largest avalanches (Takeuchi, Mineshige & Negoro 1995) at $r_{\rm tr}$. However, it should be noted that the break frequency depends not only on the size of the ADAF region but also on the propagation speed of the perturbation (Mineshige, private communication). Since the perturbation velocity should be less than the free-fall velocity, the free-fall velocity gives an upper limit to the size of the ADAF region. Thus, equation (13) of Takeuchi et al. (1995) gives an upper limit to $r_{\rm tr}$ [$r_{\rm tr} < 10^{3.2}\ (f_{\rm break}\ M_{\rm X})^{-2/3}$]. Thus, the break frequency observed in J1118+80 during outburst corresponds to $r_{\rm tr} < 5250$. The SED fits give $r_{\rm tr} \sim 350$, which is similar to the value determined from the QPO to within a factor of 2; note that the variability/QPO could have a characteristic time-scale given by a multiple of the Keplerian rotation period at $r_{\rm tr}$.

Fig. 8 shows $r_{\rm tr}$ versus the bolometric X-ray luminosity (Campana & Stella 2000) for the sources listed in Table 3. One can see that there does exist a correlation (the correlation coefficient is -0.96) with a slope index of ~ -3.0. However, more observations of $r_{\rm tr}$ during different X-ray states are required.

ACKNOWLEDGMENTS

TS, JC and CZ acknowledge support from the Spanish Ministry of Science and Technology under the grant AYA 2007–66887. Partially funded by the Spanish MEC under the Consolider-Ingenio 2010 Program grant CSD2006-00070: 'First Science with the GTC' (http://www.iac.es/consolider-ingenio-gtc/). ULTRACAM is supported by STFC grant PP/D002370/1.

REFERENCES

Blair W. P., Raymond J. C., Dupree A. K., Wu C.-C., Holm A. V., Swank J. H., 1984, ApJ, 278, 270
Campana S., Stella L., 2000, ApJ, 541, 849
Cantrell A. G., Bailyn C. D., McClintock J. E., Orosz J. A., 2008, ApJ, 673, L159
Cardelli J. A., Clayton G. C., Mathis J. S., 1989, ApJ, 345, 245
Casares J., Martin E. L., Charles P. A., Molaro P., Rebolo R., 1997, New Astron., 1, 299
Charles P. A., Coe M., 2006, in Lewin W. H. G., van der Klis M., eds, Compact Stellar X-ray Sources. Cambridge Univ. Press, Cambridge, p. 215
Chaty S., Haswell C. A., Malzac J., Hynes R. I., Shrader C. R., Cui W., 2003, MNRAS, 346, 689
Cheng F. H., Horne K., Panagia N., Shrader C. R., Gilmozzi R., Paresce F., Lund N., 1992, ApJ, 397, 664
Chevalier C., Ilovaisky S. A., van Paradijs J., Pedersen H., van der Klis M., 1989, A&A, 210, 114
Crosby N. B., Aschwanden M. J., Schmitt J. H. M. M., 1993, Sol. Phys., 143, 275
Dhillon V. et al., 2007, MNRAS, 378, 825
Esin A. A., McClintock J. E., Narayan R., 1997, ApJ, 489, 865
Esin A. A., McClintock J. E., Drake J. J., Garcia M. R., Haswell C. A., Hynes R. I., Muno M. P., 2001, ApJ, 555, 483
Fukugita M., Ichikawa T., Gunn J. E., Doi M., Shimasaku K., Schneider D. P., 1996, AJ, 111, 1748
Gelino D. M., Harrison T. E., McNamara B. J., 2001, AJ, 122, 971
Hameury J.-M., Lasota J.-P., McClintock J. E., Narayan R., 1997, ApJ, 489, 234
Hynes R. I., Mauche C. W., Haswell C. A., Shrader C. R., Cui W., Chaty S., 2000, ApJ, 539, L37
Hynes R. I., Charles P. A., Casares J., Haswell C. A., Zurita C., Shahbaz T., 2003a, MNRAS, 340, 447
Hynes R. I. et al., 2003b, MNRAS, 345, 292
Hynes R. I. et al., 2004, ApJ, 611, L125
McClintock J. E. et al., 2001, ApJ, 555, 477
Misra R., 1999, ApJ, 512, 340
Narayan R., McClintock J. E., Yi I., 1996, ApJ, 457, 821
Narayan R., Barret D., McClintock J. E., 1997, ApJ, 482, 448
Press W. H., Teukolsky S. A., Vetterling W. T., Flannery B. P., 1992, Numerical Recipes, 2nd edn. Cambridge Univ. Press, Cambridge
Shahbaz T., Dhillon V. S., Marsh T. R., Zurita C., Haswell C. A., Hynes R. I., Charles P. A., Casares J., 2003, MNRAS, 346, 1116
Shahbaz T., Hynes R. I., Charles P. A., Zurita C., Casares J., Haswell C. A., Araujo-Betancor S., Powell C., 2004, MNRAS, 354, 31
Shahbaz T., Dhillon V. S., Marsh T. R., Casares J., Zurita C., Charles P. A., Haswell C. A., Hynes R. I., 2005, MNRAS, 362, 975
Sutaria F. K. et al., 2002, A&A, 391, 993
Takeuchi M., Mineshige S., 1997, ApJ, 486, 160
Takeuchi M., Mineshige S., Negoro H., 1995, PASJ, 47, 617
Tanaka Y., Shibazaki N., 1996, ARA&A, 34, 607
Timmer J., Koenig M., 1995, A&A, 300, 707
Torres M. A. P., Casares J., Martínez-Pais I. G., Charles P. A., 2002, MNRAS, 334, 233
van der Klis M., 1994, ApJS, 92, 511
Vaughan S., 2005, A&A, 431, 391
Wijnands R., van der Klis M., 1999, ApJ, 514, 939
Zurita C. et al., 2002, MNRAS, 333, 791

This paper has been typeset from a TEX/LATEX file prepared by the author.